Bioelectrochemistry 149 (2023) 108308

Contents lists available at ScienceDirect

Bioelectrochemistry

journal homepage: www.journals.elsevier.com/bioelectrochemistry

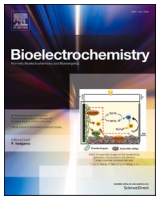

Concentration and diffusion of the redox probe as key parameters for label-free impedimetric immunosensing

Karel Lacina [a,*], Jakub Věžník [a,b], Jakub Sopoušek [a,c], Zdeněk Farka [a,c], Veronika Lacinová [d], Petr Skládal [a,c,*]

[a] CEITEC – Central European Institute of Technology, Masaryk University, Kamenice 5, Brno 625 00, Czech Republic
[b] Department of Chemistry, Faculty of Science, Masaryk University, Kamenice 5, Brno 625 00, Czech Republic
[c] Department of Biochemistry, Faculty of Science, Masaryk University, Kamenice 5, Brno 625 00, Czech Republic
[d] Department of Econometrics, Faculty of Military Leadership, University of Defence, Šumavská 4, Brno 662 10, Czech Republic

ARTICLE INFO

Dedicated to Professor Frieder W. Scheller on the occasion of his 80th birthday.

Keywords:
Electrochemical biosensor
Electrochemical impedance spectroscopy
Immunosensor
Diffusion layer
Nanopore
Polystyrene nanoparticle

ABSTRACT

Nanoporous surfaces are promising for label-free electrochemical biosensing. We formed nanopores directly on the electrode surface by means of assembling a dense layer of nonconductive nanoparticles. In our model affinity biosensor, covalent attachment of albumin protein on top of 40 nm polystyrene nanoparticles represented a capture of an analyte, resulting in blockage of the nanopores. Different bulk concentrations of the ferro/ferricyanide redox pair were probed by Faradaic electrochemical impedance spectroscopy and fast chronoamperometry. The character of the redox probe permeation towards the electrode surface differed in dependence on its concentration. These data were compared with the theoretical behavior of the free diffusion according to the Cottrell equation. Both the bulk concentration of the redox probe and the timescale of the experiment affected the performance of the electrochemical detection, demonstrating the importance of controlling these parameters in immunosensing applications.

1. Introduction

The majority of affinity electrochemical biosensors (especially immunosensors) aiming at real practice adopted concepts of enzyme-linked immunosorbent assay (ELISA) [1]. The first – capture – antibody is immobilized onto the electrode surface and binds an analyte from solution. The second – labelling – antibody is most commonly modified with a covalently linked enzyme, but also other types of labels can be used (fluorophores, nanoparticles, redox-active tags, etc.). The labelled detection antibody is utilized to generate and amplify the signal, which correlates with the analyte concentration. These systems are robust, well established, and reliable. However, multiple-step procedures are typically involved together with large benchtop instruments, which complicates the simple application in the field of point-of-care and home-care biosensing. For these reasons, other techniques and procedures are sought in order to simplify the assay format and make it more user-friendly. The label-free electrochemical biosensing based on the smart design of sensing layers is one of the possibilities.

Label-free, in our context, means biosensing without covalent labelling of any interacting (bio)molecule [2–4]. The redox probe – an electrochemically active compound – is present and freely diffuses through the solution bulk. Such biosensor thus works as a Faradaic label-free immunosensor – the measured signal is proportional to the amount of the redox probe electrochemically converted (reduced or oxidised) on the electrode; the access of the redox probe to the electrode reflects the extent of the affinity interaction occurring on its surface.

Electrochemical impedance spectroscopy (EIS) is nowadays a popular electroanalytical technique and a favourite choice for electrochemical biosensing, especially in academic research [5,6]. Throughout the literature, electrodes are being modified with analyte-specific ligands, usually proteins, and impedance is measured in the presence of the ferro/ferricyanide pair $[Fe(CN)_6]^{4-/3-}$, which acts as the most common redox probe. Its permeation through the modification layers on the electrode surface is influenced by changes in these layers. It is expected that the capture of the analyte, usually another protein, causes an increase of the impedance as proteins are generally considered to be nonconductive and are imagined only as an intact mass blocking the

* Corresponding authors at: CEITEC – Central European Institute of Technology, Masaryk University, Kamenice 5, Brno 625 00, Czech Republic (P. Skládal).
E-mail addresses: lacinak@chemi.muni.cz (K. Lacina), skladal@chemi.muni.cz (P. Skládal).

https://doi.org/10.1016/j.bioelechem.2022.108308
Received 10 April 2022; Received in revised form 15 October 2022; Accepted 15 October 2022
Available online 5 November 2022

electrode surface [7,8]. Therefore, it is anticipated that the "mass-transfer" effect exclusively governs the impedimetric response as ions permeate towards/from the electrode through these adjacent layers. However, since proteins and other biomolecules possess many (de) protonatable groups, they are certainly charged in aqueous environments [7,9,10]. Thus, the effects of charge interactions must not be overlooked.

Our recent reports [11–13] confirmed and proved that the charge of immobilized molecules on the electrode surface does play a significant role and affects the measured signal. In other words, the ionic interactions of the involved molecules affect the output of impedimetric measurements (as can be expected in electrochemistry…). Incidentally, this was also observed in the electrolyte consisting of 5 mM ferro/ferricyanide and 10 mM phosphate-buffered saline, i.e., conditions broadly employed in electroanalytical reports.

For label-free electrochemical biosensing, we designed a sensing surface based on nanopores [12,14] formed within the layer of densely (hexagonally) packed nonconductive nanoparticles (NP) deposited on the electrode surface in a planar arrangement, Fig. 1. Similar approach was also reported [15]; here, the authors have chosen different electroanalytical method and larger particles (500 and 200 nm) in comparison to the expected dimensions of biomolecules. When immobilized NPs become modified with an antigen, the electrode can act as an affinity biosensor. Exposing thus modified electrode to the solution of complementary antibodies (corresponding to the analyte in serological biosensors), the captured antibodies will hinder the permeation of the signal-generating redox probe through the blocked nanopores. However, our nanopores do not work as simply as expected – the penetration of the redox probe is extensively affected by the charge of all participating components [11,12,14]. The useful signal can be extracted from the raw measured data, and the proposed concept can be employed for affinity biosensing [12].

Such surfaces probed by EIS exhibit electrochemical behaviour described by the Randles equivalent circuit [14]. Next to solution resistance, Warburg impedance, and double layer capacitance, this circuit typically involves resistance and capacitance (RC) components, which describe charge transfer resistance with double-layer capacitance representing the solution/electrode interface. If more than one layer of NPs is employed, additional RC components appear corresponding to the interface of nanoparticles/solution, which is in that case moved farther from the electrode surface [14]. The first pair of RC components then corresponds to the interface of electrode/NPs, and the additional RC combination (new one) represents the interface of NPs/solution.

From the described behaviour, it is clear that the complexity of all interactions within the modification layers influences the permeation of the redox probe towards the electrode surface. This is fundamental for such systems. However, the rate of the redox probe permeation is also influenced by its bulk concentration. These parameters influencing the performance of nanoporous-based sensing devices have not been studied in depth yet.

For this reason, we decided to study here the model immunosensor with open and blocked nanopores at different concentrations of redox probe ferro/ferricyanide. The pores of the layer made of the 40 nm polystyrene nanoparticles modified with bovine serum albumin (BSA) were employed as the model immunoaffinity system. Covalent attachment of BSA represented a capture of an analyte, resulting in blocking the nanopores. EIS complemented with chronoamperometry were chosen as electroanalytical methods. Frequency (sampling time)-dependent differences were observed for varying redox probe concentrations. We performed an empirical analysis of the general behaviour with respect to whether this experimental condition can affect any of the analytical parameters of the developed method, such as sensitivity or instrumental requirements.

Note: in previously published immunosensing reports [12,14], one interacting partner antigen was bound on the sensing surface, and the system was designed in a way that nanopores were still open at this point. After capturing the complementary partner - antibody, nanopores were blocked. The main aim of the current paper was the more detail explanation of the effect of experimental conditions, focusing especially on the concentration of redox probe with respect to time-domain of the electroanalytical technique.

2. Experimentals

2.1. Modification of the electrodes

The electrodes of our design based on printed circuit boards were manufactured by the company Printed (www.printed.cz, Czech Republic). A photo of the electrodes can be seen in Figure S1 in the Supporting Information. The electrodes were designed in biamperometric setup [16–18] – two identical gold disks (i.d. of 0.9 mm, determined electroactive area of 1.01 mm^2 [11], separation approx. 0.5 mm apart) without any additional reference or counter electrodes. The benefits of this setup with regard to impedimetric measurements were described elsewhere [18].

The electrodes were modified according to our previously published protocol [12]. Briefly, the electrodes were polished with 50 nm alumina slurry on MicroCloth (Buehler, USA) and then treated with the solution of 0.5 M KOH and 20% H_2O_2 for 10 min to introduce a reproducible oxidized surface. Washing the electrodes with deionized water and removing any liquid residues using compressed air followed each modification step. For the majority of incubation steps, 10 mM phosphate buffer pH = 7.4 with 140 mM NaCl was employed (designated as 10/140 PBS). Thereafter, the electrodes were incubated with the solution of 50 μg/mL poly-L-lysine (Merck, www.sigmaaldrich.com) in 10/140 PBS for 30 min. A drop of 1% w/v solution of 40 nm carboxylated polystyrene nanoparticles (Magsphere, USA, https://www.magsphere.com) in 10/140 PBS was applied onto the electrodes for 30 min. Nanoparticles (NP) bind onto the poly-L-lysine provided surfaces *via* ionic attraction (poly-L-lysine is positively charged, carboxylated NPs are negatively charged [14]). Excess nanoparticles were rinsed off with distilled water, leaving only nanoparticles directly contacting the poly-L-lysine layer. Thus, a single layer of particles was obtained. In the next step, EDC/sulfo-NHS chemistry was employed to covalently cross-link

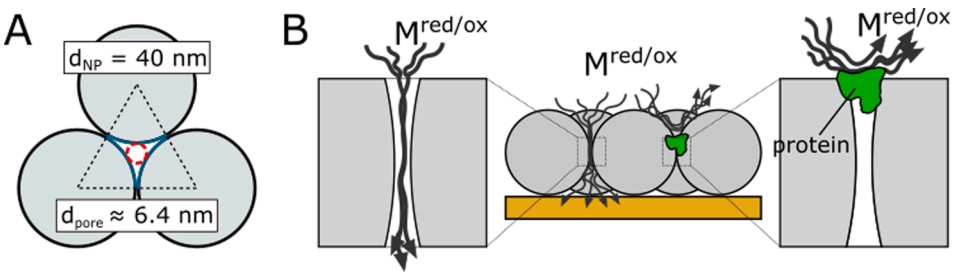

Fig. 1. Assembled nanoparticles form nearly triangular nanopore inbetween (A). Schematic representation of the function of the nanopore – after biding of the protein molecule (analyte), the nanopore is blocked, and the permeation of the redox probe ($M^{red/ox}$) to the electrode surface is hindered (B).

NPs with the underlying poly-L-lysine layer and to activate residual carboxyl groups facing the solution bulk (EDC: 1-ethyl-3-carbodiimide hydrochloride, sulfo-NHS: *N*-hydroxysulfosuccinimide). A solution of 50/50 mM EDC/sulfo-NHS (Merck) in 100 mM MES buffer (2-(*N*-morpholino)-ethanesulfonic acid/NaOH) of pH = 5.6 was applied for 20 min. The MES buffer is used for EDC/sulfo-NHS chemistry as it provides optimal pH range for carboxylic acid activation and the molecule of the MES buffer does not possess any possibly interfering chemical groups. PBS was chosen for its good buffering capacity in the range of neutral pH values. After rinsing with water, activated layer of NPs was exposed to protein (bovine serum albumin, 100 μg/ml in PBS) in the MES buffer for 60 min and incubated on a microtiter plate shaker at 250 rpm.

2.2. Electrochemical impedance spectroscopy and chronoamperometry

Electrochemical measurements were carried out using the PGSTAT302N Autolab system (Metrohm-Autolab, The Netherlands). Thanks to the planar design of the electrodes, a 6 μL droplet of solution pipetted onto the electrode area was sufficient for the measurement. The solutions of 0.5, 5, 50, and 500 mM ferro/ferricyanide redox probe in 50 mM phosphate buffer with 150 mM NaCl, pH = 7.4 (50/150 PBS) were used. All concentration points were measured in duplicates using two electrodes.

In EIS, logarithmic distribution of 20 individual frequencies from 100 000 to 2 Hz with 10 mV amplitude of potential were applied. In chronoamperometry, four 30 ms pulses of 200 mV were applied (odd pulses were positive, even ones negative). Each concentration point was measured at least twice, the obtained curves were averaged, and the second positive pulse (third in total) was evaluated.

Only a single measurement sequence (consisting of one impedimetric spectrum followed by one cycle of chronoamperometry) was performed with each electrode to eliminate the possible influences of repetitive measurements [19]. Each used electrode was discarded afterward.

3. Results and discussion

3.1. Monitoring nanopore blocking effect using electrochemical impedance spectroscopy at different redox probe concentrations

For the purpose of point-of-care label-free electrochemical biosensing using nanopores, we developed and studied in depth a system where a dense arrangement of nonconductive NPs formed nanopores (i.e., the interstitial space) directly on the electrode surface [12,14]. We have chosen electrochemical impedance spectroscopy in the Faradaic regime as the detection technique. In this technique, the whole spectrum of frequencies is typically probed [5]. However, it can be expected that not the whole spectrum will be employed in point-of-care impedimetric biosensing, and only some discrete frequency or narrow interval of frequencies will be measured. Thus, we have to ask, which frequency (or frequencies) should be used for analytical purposes.

To answer this question, we performed experiments in the system where covalent attachment of bovine serum albumin on top of 40 nm polystyrene NPs served as a model of analyte capture in affinity biosensors. In this case, surface covered with 40 nm NPs contains nanopores of approx. 6.4 nm, and these should be "fully" blocked when BSA molecule binds in their close proximity [12]. Moreover, the overall charge of BSA molecule in physiological pH of 7.4 is rather negative [13]. Thus, the measured impedance is expected to increase significantly.

Fig. 2A shows the EIS data measured with open and blocked nanopores. The values of real impedance *Z*' were plotted against the frequency of potential perturbation. Absolute impedances exhibited similar trends, but one particular phenomenon was better visible on the plot of real impedance, as will be described further (see Figures S2 and S3 in Supporting Information for additional data and corresponding Nyquist plots; note: as we focused rather on the real part of impedance herein, one should be aware that other information from the imaginary parts were not considered). Each dataset consists of at least two electrodes which responses were averaged. The concentration of the redox probe was studied as the main variable. With the increasing redox probe concentration, the measured impedance of both open and blocked nanopores decreased due to the higher conductivity of the solution and especially due to the higher Faradaic currents (Fig. 2A). From the comparison of pair of curves at a particular concentration of [Fe

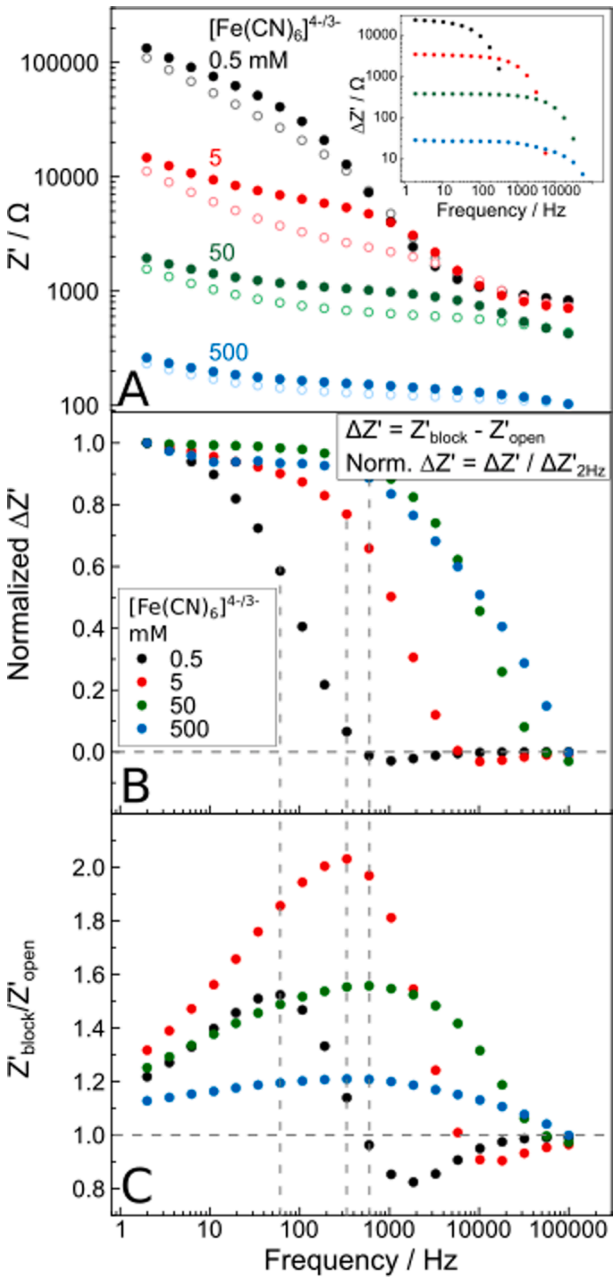

Fig. 2. EIS of open (open circles) and blocked (full circles) nanopores at 0.5, 5, 50, and 500 mM $[Fe(CN)_6]^{4-/3-}$. A real part of impedance was evaluated and plotted against frequency. Each dataset represents an average of two disposable electrodes, each measured only once. Inset: Plot of subtracted data $Z'_{block}-Z'_{open}$ before normalization. (A) Subtracted data after normalization using the value of the difference of real impedance of blocked and open pores at the frequency of 2 Hz. The "useful range" (see main text for details) of frequencies widens with the redox probe concentration. (B) The ratio of impedances of blocked and open nanopores. Dashed vertical lines highlight the "optimal analytical" frequencies for particular redox probe concentrations using our experimental setup. (C).

$(CN)_6]^{4-/3-}$, the increase of the impedance for blocked nanopores is apparent (difference from open to full circles).

The differences between bare NPs and those modified with BSA were subtracted (inset of Fig. 2A). However, for a better visibility, these values were normalized using the value of the difference of the blocked and open nanopores at the frequency of 2 Hz ($[Z'_{block} - Z'_{open}]/[Z'_{block,\ 2\ Hz} - Z'_{open,\ 2\ Hz}]$, the frequency of 2 Hz was employed for the normalization, because changes of signal at this frequency are almost exclusively in the real part of impedance Z'). As shown in Fig. 2B, the useful range of frequencies is widened towards higher frequencies with increasing redox probe concentration. By the "useful range", we understand the range of frequencies where the increase of electrochemical impedance for blocking the pores is observable, i.e., it is increased above zero. This result means that at higher redox probe concentration, a wider range of frequencies or any discrete value from this range can be used to monitor the analytical event (analyte binding).

When the original raw data of blocked and unoccupied nanopores are put directly into a ratio (Z'_{block}/Z'_{open}, Fig. 2C), another analytical aspect can be evaluated – the relative magnitude of the increase of impedance for blocking the pores. Thus, in this case, the sensitivity of the measuring technique is the parameter of interest. From this point of view, the most promising concentration of redox probe seems to be 5 mM, as the ratio is the highest at frequencies just above 300 Hz (red data points in Fig. 2C).

It can be concluded from the experiment that each concentration of $[Fe(CN)_6]^{4-/3-}$ does not only provide a suitable interval of useful frequencies but provides also one "optimal analytical" frequency. The optimal analytical frequency is meant as the frequency at which the ratio of impedance of blocked pores to impedance of open pores is highest. As can be seen in Fig. 2C, these are 60, 335, 585, and 585 Hz for concentrations of 0.5, 5, 50, and 500 mM, respectively. It must be stressed that these values are highly dependent on the setup, and other experimental parameters (e.g., ionic strength and charge of biomolecules [13]) can affect the electrochemical behavior.

An interesting phenomenon can be observed for a specific range of higher frequencies – the impedance of blocked nanopores is lower than that of open ones. This is apparent in whole Fig. 2, but best visible in Fig. 2C for lower concentrations of $[Fe(CN)_6]^{4-/3-}$. Probably, the redox probe present under the blocked nanopore is encapsulated, and at higher frequencies, its electrochemical conversion is more rapid and efficient as it cannot diffuse out through the pore towards the bulk.

3.2. Monitoring nanopore blocking using chronoamperometry at different redox probe concentrations

The same experimental setup was also monitored using chronoamperometry. In Fig. 3A, an exemplary trace of the measurement in 50 mM $[Fe(CN)_6]^{4-/3-}$ is shown. Measurements performed with other concentrations are provided in Figures S4–7 in the Supporting Information. Open nanopores (dashed line) exhibited higher currents as the redox probe can reach the electrode surface easily without further obstacles (not considering the layer of NPs). On the other hand, blocking the nanopores with protein (dotted line) causes the decrease of the measured current as the access to the electrode surface is hindered. The difference between open and blocked nanopores is visualised as a solid line. Note that this difference is calculated in the opposite manner than in impedance measurements; the value of blocked nanopores is subtracted from the value of open pores.

At closer inspection of Fig. 3A, the formation of the transient double layer at the interface of electrode/solution influences the current response of the first pulse, which differs from all subsequent pulses – its absolute magnitude is lower. From the second pulse (first negative), the measurement-dependent double layer above the electrode is established, and differences in absolute signal between further pulses are negligible. In addition, return to the pre-measurement state (1:1 ratio of $[Fe(CN)_6]^{4-}$: $[Fe(CN)_6]^{3-}$ above the electrode) is visible in the last section where the potential of 0 V was applied, and still the current from the double layer reformation was measured (marked with an arrow). The third pulse of potential (second positive) was further evaluated.

In Figure 3B, a different course of signal traces for the different concentrations of redox probe is apparent. In other words, diffusion of the redox probe through the nanopores layer exhibited a different character. Again, the data measured at different redox probe concentrations first had to be normalized to be comparable. The difference of open and blocked pores was normalized by the first point (highest value) of the open-pore signal (see the inset of Fig. 3B for schematic visualization). From the presented data, no regular trend in the behaviour can be deduced at first glance. Only discrete values of "the best performance" – the most significant difference – are visible for the selected values of time – 5 mM at 0.1 ms, 50 mM at 5 ms, and 500 mM at 30 ms (circled points in Fig. 3B).

Since we suspected different diffusion of the redox probe to cause the majority of the differences in the measured signal, the raw chronoamperometry data were further compared with traces of the theoretical current according to the Cottrell equation (Fig. 3C):

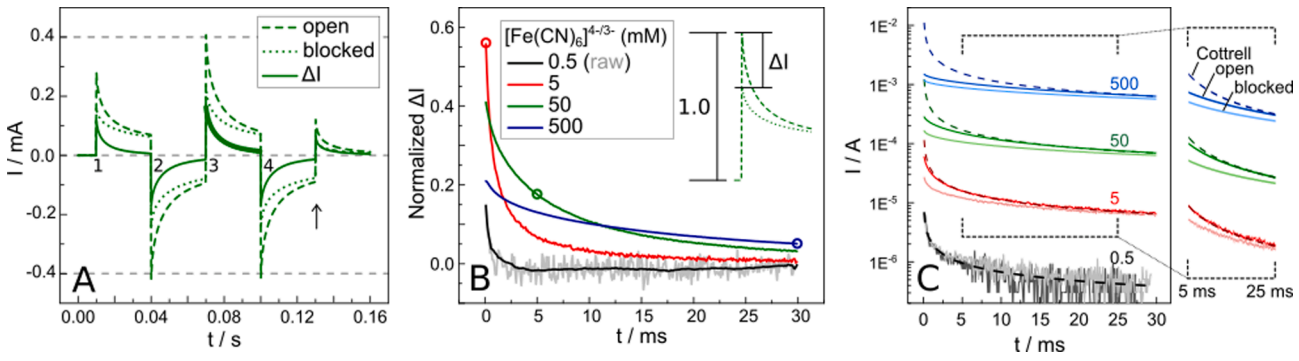

Fig. 3. Chronoamperometry signal traces in 50 mM ferro/ferricyanide – open (dashed line) and blocked (dotted line) nanopores, subtracted signal $\Delta I = I_{open} - I_{blocked}$ (solid line). Switching potentials were +/- 200 mV. Numbers 1–4 address particular pulses of potential. Application of the zero potential at the end of the measurement cycle is marked with an arrow. (A) Comparison of normalized signals of the third pulse of potential (second positive pulse, highlighted in (A) with thicker line) at different redox probe concentrations. Normalization was done according to the inset – subtracted signals were normalized by the highest signal (first point) of open pores. Data points at particular time values of 0.1, 5, and 30 ms, which are further discussed in the text, are highlighted as coloured circles. The lowest concentration was smoothed as the raw (grey) signal was very noisy. (B) Comparison of signal traces for open, blocked nanopores, and theoretical current according to the Cottrell equation for 0.5, 5, 50, and 500 mM $[Fe(CN)_6]^{4-/3-}$. On the right, zoom of signal traces of 5, 50, and 500 mM concentrations in the time period between 5 and 25 ms are shown for better visualization. The lowest concentration of the redox probe of 0.5 mM was not included due to the noisy signal. (C).

$$i = \frac{nFAc\sqrt{D}}{\sqrt{\pi t}} \quad (1)$$

where (1) F and t represent Faraday constant and time, respectively, only one electron was transferred (n), and the diffusion coefficient D was considered $6.67 \cdot 10^{-6}$ cm^2/s for ferrocyanide that is oxidized during the positive pulse of potential [20]. The active area of clean unmodified electrode A was previously determined to be 1.01 mm^2 [11]. The actual area blocked by nonconductive spherical nanoparticles is dependent on their deformation, but based on the electrochemical data, it was here empirically estimated to be one third of the determined active surface of an unmodified electrode (the estimated area was even lower for the concentration of 0.5 mM – approx. 25%). In Fig. 3C, the course of the theoretical current given by the Cottrell equation is represented by the dashed curve for each concentration.

Several observations can be made. Generally, the theoretical curve corresponds in a greater extent to the signal trace measured with open pores (the upper curve from the pair of the experimental traces for each concentration). At the lowest concentration of the redox probe of 0.5 mM, the curve of theoretical current and both measured signals (open and blocked pores) are more or less overlapping throughout the whole experiment, and this concentration point was not further analysed due to its noisy and poorly reproducible signal. For a concentration of 5 mM, all three curves overlap at the end of the potential pulse (above 25 ms). A slight difference between theoretical and open-pore curves is visible at the beginning of the measurement. This difference is more prominent with higher concentrations. Furthermore, the difference between blocked and open pores is firstly observable at the beginning of this concentration, 5 mM $[Fe(CN)_6]^{4-/3-}$, and this difference is widened through the whole pulse of potential with the increasing redox probe concentration. At 500 mM, the difference is nearly constant throughout the whole 30 ms; in other words, the traces of open and blocked pores are almost parallel in this case.

Although mainly faradaic currents given by the diffusion of the redox probe are suspected from the change of the signal of open and closed nanopores, some influence of capacitive currents can not be ruled out (see measurement with open pores in PBS in Figure S8). However, the capacitive currents are decreasing with the increasing concentration of the redox probe (Figure S3) and the deviation between the measured current and the fit according to the Cottrell equation in chronoamperometry is bigger for higher concentrations of the redox probe. For these reasons, we assume that the differences between experimental results of open and closed pores and fitted data are mainly caused by the differently extended diffusion layer above the electrode surface after the application of the pulse of potential. This agrees with observations made in EIS measurements that the applicable range of frequencies was widened at the higher redox probe concentrations. However, comprehensive impedimetric analysis of the system (including also imaginary part of impedance) is necessary to confirm these assumptions.

3.3. Detection method for electrochemical label-free biosensing

In the literature, it is sometimes disputed "which electrochemical method is better for label-free immunosensing" [21]. To discuss this further, one point should be stated. We assume that in such a specific electroanalytical task, the rate of the redox probe conversion on the electrode surface should be "constant", and only changes in its permeation through the upper parts of the modification layer where the analyte is being bound should be sensed.

Measurement of the Faradaic electrochemical impedance can be directly compared to a voltammetric technique – its absolute magnitude can be quantified from the ratio of applied potential and measured current (irrespective of its delay after excitation signal for now). If not talking about amplitude, though important, frequency of EIS can be related with time-domain of other potentiostatic methods [6] and so with a scan rate of cyclic voltammetry where the time domain is in addition related with potential (f [Hz] $= 1/t$ [s^{-1}] $\approx \nu$ [$mV.s^{-1}$]). For example, current measured in EIS at a frequency of 1 Hz and amplitude of 10 mV is analogous to the first second of chronoamperometry with a potential pulse of 10 mV and to the cyclic voltammetry with a scan rate of 10 mV/s. In other words, each time point (with its measured current/potential or resistance) can be expressed as a specific concentration gradient profile of the redox probe above the electrode and should give comparable results regardless of the adopted measuring technique.

This is visible not only [6] from our presented results. Although differently set, EIS together with chronoamperometry gives comparable results at comparable conditions (redox probe concentration, readout time). This does not mean that other methods are useless and also this does not imply that any of these methods is better. For example, cyclic voltammetry is irreplaceable for probing unknown systems, and amperometric methods are remarkable for their sensitivity and simplicity of the detection devices. However, if a defined analytical task with a fully described, established, and controlled analytical procedure is considered (e.g., label-free electrochemical biosensing), then it does not matter which of these electroanalytical methods is used as a detection technique.

4. Conclusions

In this contribution, we studied the decisive parameters for the performance of electrochemical impedance spectroscopy, especially the effect of concentration of redox probe with respect to time domain of the electroanalytical technique.

We already know that the redox probe can interact with charged entities within the modification coating on the electrode surface [11]. In the current work, we observed the crucial role of the diffusion layer above the electrode. This was studied by controlling the bulk concertation of ferro/ferricyanide from 0.5 up to 500 mM, consequently changing also its local concentration above the electrode surface.

From our results, one can conclude that the output of the detection technique is related to both the timescale of the experiment and the concentration of the redox probe (concentration profile at the electrode surface); however, there is not only a single optimal readout combination. Demands on the analytical method can be different for each analytical task. For example, in our case, the optimal conditions can be either 5 mM of the redox probe at 330 Hz for the most sensitive output or >50 mM concentration for the least instrument demanding setup – any value from 2 Hz up to 10 000 Hz can be employed for simplified single-frequency sensing.

We assume that proper tuning of the diffusion layer can influence the performance of the label-free electrochemical (impedimetric) affinity biosensors. This behaviour will be studied in more detail in the future.

Declaration of Competing Interest

The authors declare that they have no known competing financial interests or personal relationships that could have appeared to influence the work reported in this paper.

Data availability

Data will be made available on request.

Acknowledgement

This research has been financially supported by the Ministry of Education, Youth, and Sports of the Czech Republic under the project CEITEC 2020 (LQ1601), by the Czech Science Foundation, grants no. 19-16273Y and 21-03156S, and by the Ministry of Health of the Czech Republic, grant no. NU20-08-00106.

Appendix A. Supplementary data

Supplementary data to this article can be found online at https://doi.org/10.1016/j.bioelechem.2022.108308.

References

[1] C.A. Marquette, L.J. Blum, State of the art and recent advances in immunoanalytical systems, Biosens. Bioelectron. 21 (2006) 1424–1433, https://doi.org/10.1016/j.bios.2004.09.037.

[2] J.S. Daniels, N. Pourmand, Label-Free Impedance Biosensors: Opportunities and Challenges, Electroanalysis. 19 (2007) 1239–1257, https://doi.org/10.1002/elan.200603855.

[3] D.N. Mazaafrianto, A. Ishida, M. Maeki, H. Tani, M. Tokeshi, Label-Free Electrochemical Sensor for Ochratoxin A Using a Microfabricated Electrode with Immobilized Aptamer, ACS Omega 3 (2018) 16823–16830, https://doi.org/10.1021/acsomega.8b01996.

[4] S. Yang, F. Zhang, Z. Wang, Q. Liang, A graphene oxide-based label-free electrochemical aptasensor for the detection of alpha-fetoprotein, Biosens. Bioelectron. 112 (2018) 186–192, https://doi.org/10.1016/j.bios.2018.04.026.

[5] F. Lisdat, D. Schäfer, The use of electrochemical impedance spectroscopy for biosensing, Anal. Bioanal. Chem. 391 (5) (2008) 1555–1567.

[6] S. Wang, J. Zhang, O. Gharbi, V. Vivier, M. Gao, M.E. Orazem, Electrochemical impedance spectroscopy, Nat. Rev. Methods Primer. 1 (2021) 41, https://doi.org/10.1038/s43586-021-00039-w.

[7] Y. Ram, T. Yoetz-Kopelman, Y. Dror, A. Freeman, Y. Shacham-Diamand, Impact of molecular surface charge on biosensing by electrochemical impedance spectroscopy, Electrochim. Acta 200 (2016) 161–167, https://doi.org/10.1016/j.electacta.2016.03.162.

[8] X. Cui, R. Pei, Z. Wang, F. Yang, Y. Ma, S. Dong, X. Yang, Layer-by-layer assembly of multilayer films composed of avidin and biotin-labeled antibody for immunosensing, Biosens. Bioelectron. 18 (2003) 59–67, https://doi.org/10.1016/S0956-5663(02)00114-8.

[9] L.A. Khawli, S. Goswami, R. Hutchinson, Z.W. Kwong, J. Yang, X. Wang, Z. Yao, A. Sreedhara, T. Cano, D. Tesar, I. Nijem, D.E. Allison, P.Y. Wong, Y.-H. Kao, C. Quan, A. Joshi, R.J. Harris, P. Motchnik, Charge variants in IgG1: Isolation, characterization, in vitro binding properties and pharmacokinetics in rats, MAbs. 2 (2010) 613–624, https://doi.org/10.4161/mabs.2.6.13333.

[10] P. Ghisellini, M. Caiazzo, A. Alessandrini, R. Eggenhöffner, M. Vassalli, P. Facci, Direct electrical control of IgG conformation and functional activity at surfaces, Sci. Rep. 6 (2016), https://doi.org/10.1038/srep37779.

[11] K. Lacina, J. Sopoušek, V. Čunderlová, A. Hlaváček, T. Václavek, V. Lacinová, Biosensing based on electrochemical impedance spectroscopy: Influence of the often-ignored molecular charge, Electrochem. Commun. 93 (2018) 183–186, https://doi.org/10.1016/j.elecom.2018.07.015.

[12] J. Sopoušek, J. Věžník, P. Skládal, K. Lacina, Blocking the Nanopores in a Layer of Nonconductive Nanoparticles: Dominant Effects Therein and Challenges for Electrochemical Impedimetric Biosensing, ACS Appl. Mater. Interfaces 12 (2020) 14620–14628, https://doi.org/10.1021/acsami.0c02650.

[13] J. Sopoušek, J. Věžník, J. Houser, P. Skládal, K. Lacina, Crucial factors governing the electrochemical impedance on protein-modified surfaces, Electrochim. Acta 388 (2021), 138616, https://doi.org/10.1016/j.electacta.2021.138616.

[14] J. Sopoušek, J. Humlíček, A. Hlaváček, V. Horáčková, P. Skládal, K. Lacina, Thick nanoporous matrices of polystyrene nanoparticles and their potential for electrochemical biosensing, Electrochim. Acta. 368 (2021), 137607, https://doi.org/10.1016/j.electacta.2020.137607.

[15] A. de la Escosura-Muñiz, M. Espinoza-Castañeda, M. Hasegawa, L. Philippe, A. Merkoçi, Nanoparticles-based nanochannels assembled on a plastic flexible substrate for label-free immunosensing, Nano Res. 8 (2015) 1180–1188, https://doi.org/10.1007/s12274-014-0598-5.

[16] M. Rahimi, S.R. Mikkelsen, Cyclic Biamperometry, Anal. Chem. 82 (2010) 1779–1785, https://doi.org/10.1021/ac902383w.

[17] M. Rahimi, S.R. Mikkelsen, Cyclic Biamperometry at Micro-Interdigitated Electrodes, Anal. Chem. 83 (2011) 7555–7559, https://doi.org/10.1021/ac2012703.

[18] K. Lacina, P. Vanýsek, P. Bednář, L. Trnková, P. Skládal, Redox-Pair-Defined Electrochemical Measurements: Biamperometric Setup for Elimination of Interferent Effects and for Sensing of Unstable Redox Systems, ChemElectroChem. 3 (2016) 877–882, https://doi.org/10.1002/celc.201600076.

[19] A. Bogomolova, E. Komarova, K. Reber, T. Gerasimov, O. Yavuz, S. Bhatt, M. Aldissi, Challenges of Electrochemical Impedance Spectroscopy in Protein Biosensing, Anal. Chem. 81 (2009) 3944–3949, https://doi.org/10.1021/ac9002358.

[20] S.J. Konopka, Bruce. McDuffie, Diffusion coefficients of ferri- and ferrocyanide ions in aqueous media, using twin-electrode thin-layer electrochemistry, Anal. Chem. 42 (1970) 1741–1746. https://doi.org/10.1021/ac50160a042.

[21] L. Alfonta, A. Bardea, O. Khersonsky, E. Katz, I. Willner, Chronopotentiometry and Faradaic impedance spectroscopy as signal transduction methods for the biocatalytic precipitation of an insoluble product on electrode supports: routes for enzyme sensors, immunosensors and DNA sensors, Biosens. Bioelectron. 16 (2001) 675–687, https://doi.org/10.1016/S0956-5663(01)00231-7.